



Nature and Mechanism of the Metals Ions Adsorption from a Ternary Aqueous Medium Using Natural Sedimentary Rock

Rajaa Bassam¹ · Marouane El Alouani² · Jabrane Maissara¹ · Younes Rachdi¹ · El Hassan El Khattabi¹ · Hamid Saufi² · Mohammed El Mahi Chbihi¹ · Said Belaaouad¹

Received: 4 March 2022 / Accepted: 26 June 2022 / Published online: 16 July 2022
© The Tunisian Chemical Society and Springer Nature Switzerland AG 2022

Abstract

The objective of this study consists to investigate an efficient, and green pathway of multi-metals Cd (II), Cr (VI), and As (III) recovery from aqueous solutions by adsorption process using natural sedimentary rock (NSR) in the batch mode. This adsorbent was characterized before and after the adsorption process by several techniques i.e., X-ray diffraction (XRD), X-ray fluorescence (XRF), Fourier transform infrared (FTIR), Time-of-Flight Secondary Ion Mass Spectrometry (ToF-SIMS), Scanning Electron Microscopy with Energy-Dispersive X-ray spectroscopy (SEM/EDX), Atomic Force Microscopy (AFM), and Cation Exchange Capacity (CEC). The competitive removal process was undertaken to evaluate the effect of adsorbent mass, contact time, initial concentration, solution pH, and temperature. The kinetic data were analyzed using the linear and nonlinear forms of pseudo-first-order and pseudo-second-order kinetic models. According to the modeling of the experimental results, the adsorption kinetics was adapted to the linear pseudo-second-order model. The adsorption isotherm was evaluated by the linear and nonlinear forms of Langmuir and Freundlich isotherm models. The experimental isotherm data were better fitted with the linear Langmuir model rather than the Freundlich isotherm model. The maximum experimental adsorption capacities (Q_{max}) predicted by the Langmuir model were 16.75 mg g⁻¹ for Cr (VI), 21.45 mg g⁻¹ for As (III), and 12.63 mg g⁻¹ for Cd (II). The values of thermodynamic parameters revealed that the multi-metals removal of Cd (II), Cr (VI), and As (III) onto NSR was exothermic, favorable, and spontaneous in nature. Based on the results, this untreated rock can be used as an inexpensive adsorbent to treat water contaminated by heavy metals in the multi-metals system.

Keywords Raw rock · Characterization · Heavy metals · Competitive · Adsorption

1 Introduction

Water is an essential element in human life and its activity, such as domestic, industrial, and agricultural activities, making it a receiving element exposed to all types of pollution. Heavy metals including Cadmium (Cd), Chromium (Cr), and Arsenic (As) are among the pollutants that make up a

high risk to the environment and human health due to their resistance to biodegradability, their accumulation, and use in several sectors. Many studies in the literature reviewed to toxic effects of these metals on living organisms [1, 2]. For this reason, it is particularly important to control the water quality and the water content of heavy metals. Numerous techniques were used to treat water contaminated with heavy metals, but the adsorption by natural adsorbents is the most efficient and low-cost process to trap these metals.

Natural mineral rocks have recently received considerable attention as less expensive, non-toxic, and abundant alternative materials with multifunctional properties. Several literature studies have suggested the effectiveness of natural rocks as adsorbents for heavy metals removal [3, 4]. These rocks have numerous physicochemical properties which usually give them a high adsorption capacity thanks to the large specific surface area, and a high cation exchange capacity. Wawan Budianta investigated the removal of Cu

✉ Rajaa Bassam
bassam.rajaa@gmail.com

¹ Laboratory of Physical Chemistry of Materials LCPM, Faculty of Sciences Ben M'Sik, Hassan II University of Casablanca, Bd CdtDriss El Harti, B.P.7955, Casablanca, Morocco

² Centre des Sciences des Matériaux (CSM), Laboratoire de Physico-chimie des Matériaux Inorganiques et Organiques (LPCMIO), Ecole Normale Supérieure (ENS), Mohammed V University in Rabat, Rabat, Morocco

(II), Pb (II), Zn (II), and Cd (II) from aqueous solution using four clay samples collected from Java, Indonesia [5]. The SLM and Gk clay were mainly composed of kaolinite, but the BYL and PCT clay were dominated by montmorillonite. The maximum removal quantities of heavy metals were obtained using BYL and PCT. The recovery of Cu (II), Pb (II), and Cd (II) using natural illitic clay collected from Marrakech region in Morocco from an aqueous solution [6]. The essential compound of natural clay was illite as a principal phase with quartz. The removal capacities attached from the natural clay were 5.25 mg g^{-1} for Cd (II), 13.41 mg g^{-1} for Cu (II), and 15.90 mg g^{-1} for Pb (II) ions. The adsorption mechanism of Cu (II), Pb (II), and Cd (II) indicates that the silanol (Si–O) and aluminol (Al–Al–OH) groups were the principal groups involved in the removal of Cu (II), Pb (II), and Cd (II). The removal of Cd (II) and Co (II) by chemically modified Malangali kaolin was investigated [7]. The pore volume and the pore size of chemically modified Malangali kaolin were 0.81 cc g^{-1} and 3.60 nm , respectively. The maximum recovery capacity of Cd (II) was 1.067 mg g^{-1} and 1.043 mg g^{-1} for Co (II). This adsorption efficiency of Cd (II) and Co (II) was maybe due to the functional groups on the surface of chemically modified Malangali kaolin including the groups –OH, O–Si–O, and Al–O–Al that facilitates the binding of heavy metal ions from aqueous solutions.

The industrial effluents were typically contaminated with several pollutants that have aggravated the treatment process and reduced ecosystem protection. However, most of the work mentioned in the literature was focused on single-element systems. In this context, the present work is interested in the performance of the Cd (II), Cr (VI), and As (III) competitive elimination using raw rock. The rock used was sampled in the Middle Atlas region of Morocco, and it was selected mainly based on its different physical and chemical properties. Therefore, the characterization of the raw rock before and after the adsorption was investigated to more understand the mechanisms of the Cd (II), Cr (VI), and As (III) competitive retention. The adsorption process was influenced by different parameters including the rock mass, contact time, initial concentration, solution pH, and temperature. The kinetic, isotherm, and thermodynamic studies were also investigated. The desorption of Cd (II), Cr (VI), and As (III) was tested by using various acids.

2 Materials and Methods

2.1 Preparation and Characterization of NSR

The natural rock was collected from the Middle Atlas region of Morocco, it was referred by NSR to Natural

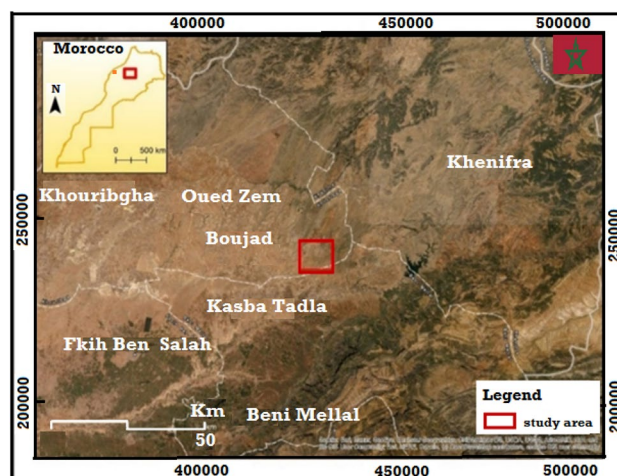


Fig. 1 Topographic map of collection site of NSR

Sedimentary Rock. The geographic map present in Fig. 1 indicates the location of this adsorbent. NSR was crushed using (FRITSCH PULVERISETTE 14) and to obtain a homogeneous and finer powder it was ground by RETSCH ZM 200 with an average particle diameter of $500 \mu\text{m}$. The characterization of NSR was performed before and after the adsorption process. The chemical and mineralogical composition is identified by X-ray diffraction (XRD) using BRUKER-binaryV4. The elemental analysis was detected by X-ray fluorescence (XRF) using EPSILON 4. The Fourier transform infrared (FTIR) was used to detect carbonates and structural groups present in the adsorbents using SHIMADZU8400S. Scanning electron microscopy coupled with energy-dispersive X-ray spectroscopy (SEM–EDX) was used to bring the detailed high-resolution images, quantitative compositional information, and elemental identification of adsorbents. The Atomic Force Microscopy (AFM) was used to determine changes in particle morphology before and after the adsorption by Agilent 5500 AFM. Time of flight secondary ions mass spectrometry (ToF–SIMS) imaging analysis was performed to provide information on the molecular and elemental species present on the surface using the Zeiss model. The cation exchange capacity (CEC) was investigated to estimate the theoretical cation fixation power using the cobalt hexamine chloride method, which consists in measuring by colorimetry the concentration of cobalt hexamine ions residual in the supernatant after the adsorption by the rock. The amount of cobalt hexamine is determined by the difference between the initial and final concentrations. In this study, the mixture of 100 mg NSR and 25 mL of cobalt hexamine ($5 \cdot 10^{-3} \text{ M}$) were agitated for 2 h then centrifuged and filtered, and the recovered filtrates were analyzed by HACH DR 6000 UV/visible spectrophotometry at $\lambda = 476 \text{ nm}$.

2.2 Adsorption Experiments

The chemical reagents used in this research were obtained from LaboChimie company, with the analytical grade, and were dissolved in double-distilled water. The removal of multi-metals Cd (II), Cr (VI), and As (III) from aqueous solution was investigated according to several parameters such as contact time, NSR mass, solution pH, temperature, and the initial concentration. The pH of the solution was adjusted by adding HCl (1 M) or NaOH (1 M). The solutions were filtered using a filter (0.45 μm) before analyzing the concentration of each metal by inductively coupled plasma mass spectrometry (ICP-MS) using the PerkinElmer model. The amount of Cd (II), Cr (VI), and As (III) adsorbed was calculated by the equation:

$$Q_e = \frac{V(C_0 - C_e)}{m} \quad (1)$$

where Q_e is the adsorbed amount (mg g^{-1}); m is the mass of NSR (g); C_0 is the initial concentration (mg L^{-1}); V is the volume of solution (mL); and C_e is the equilibrium concentration (mg L^{-1}).

2.3 Adsorption Desorption Process

The desorption process was carried out by adding of NSR containing Cd (II), Cr (VI), and As (III) in different acids including nitric acid (1 M), hydrochloric acid (1 M), and sulfuric acid (1 M). These mixtures were shaken at 450 rpm for 30 min for three cycles. After desorption, the concentrations of Cd (II), Cr (VI), and As (III) ions were analyzed using ICP-MS.

3 Results and Discussion

3.1 Characterization of NSR

3.1.1 XRF Analysis

To determine the chemical composition of NSR an analysis by X-ray fluorescence was performed. Table 1 groups the chemical composition present in the NSR sample. A high percentage of silica (SiO_2) existed in NSR with other oxides including Al_2O_3 , Fe_2O_3 , CaO, MgO, and K_2O attained a percentage ranging from 1.42 to 12.65%. The content of these oxides shows that NSR rich exchangeable elements such as Fe^{2+} , Al^{3+} , Mg^{2+} , K^+ , and Na^+ , which promotes the adsorption of heavy metals on its surface since of their affinity to these elements.

Table 1 Chemical composition of NSR analyzed by XRF

Component	SiO_2	CaO	Fe_2O_3	Al_2O_3	MgO	K_2O	Na_2O	Others
Weight (%)	64.27	3.25	11.26	12.65	6.31	1.42	0.38	0.46

3.1.2 XRD Analysis

The mineralogical composition of NSR was studied using X-ray diffraction (Fig. 2). It can be concluded that NSR mainly consists of Clinocllore which was located at 6.22° , 12.49° , 27.93° , and 40.27° . Significant phases of Albite were detected at 8.85° , 36.53° , 39.45° , and 50.11° , with a major peak of Quartz at 20.85° , 26.62° , 43.18° , 50.11° , 54.85° , 59.93° , and 68.11° . Associated with Calcite and Muscovite at 29.42° and 42.43° , respectively. From these results, it can be decided that NSR is heterogeneous, which was confirmed by the results obtained by XRF.

3.1.3 FTIR Analysis

The study of NSR using FTIR aims to assess the different chemical functions existing on the surface of NSR (Fig. 3). The absorption bands that appear at 3389 cm^{-1} and 1647 cm^{-1} correspond to the stretching and bending vibration of OH group [6, 7]. The Albite was detected in the region from 534 to 617 cm^{-1} may be owed to the stretching and bending vibration of the Si–O–Si [8, 9]. The characteristic bands of carbonates owing to C=O, C–O, and Q=C=O were detected at 1451 , 1259 , and 877 cm^{-1} due to the Calcite [9–11]. An intense band located at 1047 , 982 , and 779 cm^{-1} corresponds to Si–O stretching vibrations of Quartz [12, 13]. While the Clinocllore bands were detected at 652 , 573 , and

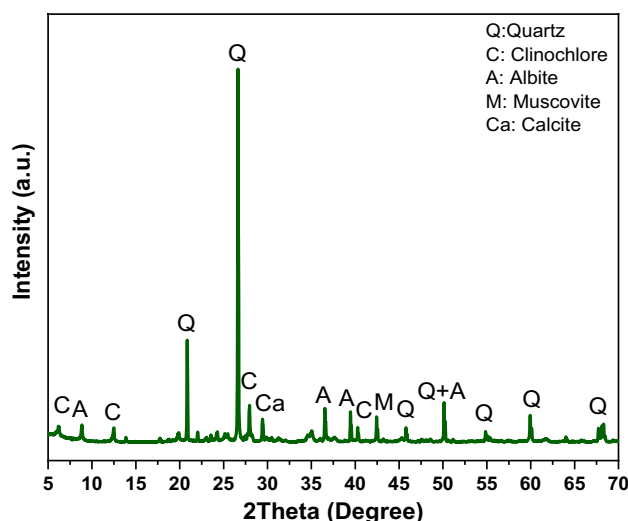


Fig. 2 XRD pattern of NSR. Clinocllore (JCPDS 00-029-0701), Albite (JCPDS 01-089-6427), Muscovite (JCPDS 00-007-0042), Quartz (01-070-3755), and Calcite (01-086-0174)

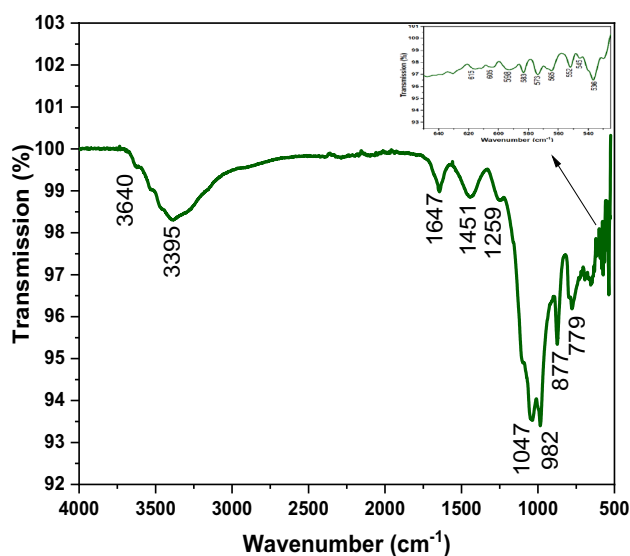


Fig. 3 FTIR spectra of NSR

552 cm^{-1} were attributed to the bending vibrations of the Si–O–Si, Fe–O, and (Fe or Mg or Al)–O–Si, respectively. The structural study of NSR was compatible with those found by XRD analysis.

3.1.4 SEM /EDX Analysis

The surface morphology of NSR was examined using SEM (Fig. 4). The SEM image shows spherical grain aggregates with a heterogeneous size. The pores were formed in the interstices between the grains. It was observed also that a big irregular form of the cavities the surface of these cavities was rich by several chemical elements composition, which confirmed the composition heterogeneous. Therefore, the EDX spectra present a high amount of oxygen, silicon, iron, aluminum, magnesium, and calcium. Other elements were presented in trace amounts including sodium and potassium. According to these results, NSR has a porous surface and functional groups on the surface.

3.1.5 ToF–SIMS Analysis

The distribution maps from ToF–SIMS provide data about the surface of the samples. Figure 5 gathers the weight of all the elements contained in NSR. TOF–SIMS maps were adapted to the previous results, they show the superficial image of the most representative ions of NSR. Therefore, the distribution maps were also observed high content of oxygen, silicon, iron, aluminum, magnesium, and calcium but to a smaller extent potassium and sodium on the surface.

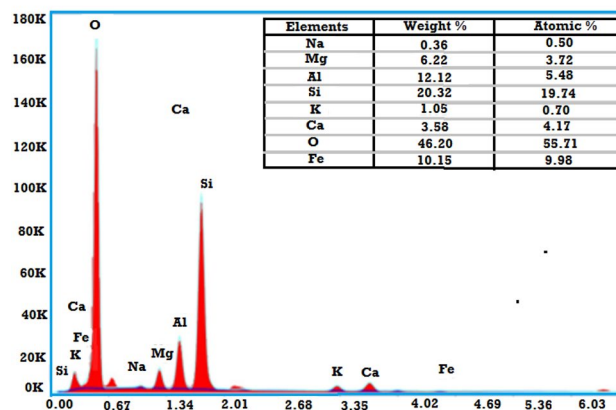
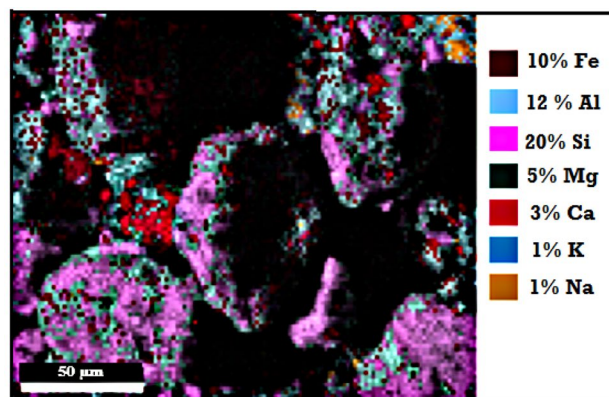


Fig. 4 SEM/EDX analysis of NSR

3.1.6 Point of Zero Charge

The point of zero charge (PZC) is the pH at which the adsorbent surface charge density is equal to zero. It is the point at which the adsorbent has load potential on its surface, the presence of OH^- ions and H^+ in the solution can change the potential of surface loads of the adsorbent using NaCl [14]. Generally, there are two types of charge in the minerals matrix, including the permanent negative charge from pH-independent isomorphous substitution and the charge of the hydroxyl groups present on the lateral faces which have a pH-dependent amphoteric character. The surface charge of the minerals particles is zero at the corresponding pH at zero charge (positive and negative charges are compensated), indicating that there are no electrostatic interactions between the particles. While at pH below pH_{PZC} , the surface load is positive, in contrast at pH above pH_{PZC} the surface takes a negative load. From Fig. 6 the PZC value of NSR was around 6.6 similar results were also found in previous studies [15]. These results showed that the surface of NSR was positively charged when the $\text{pH} < 6.6$, which limits their ability to retain cationic ions.

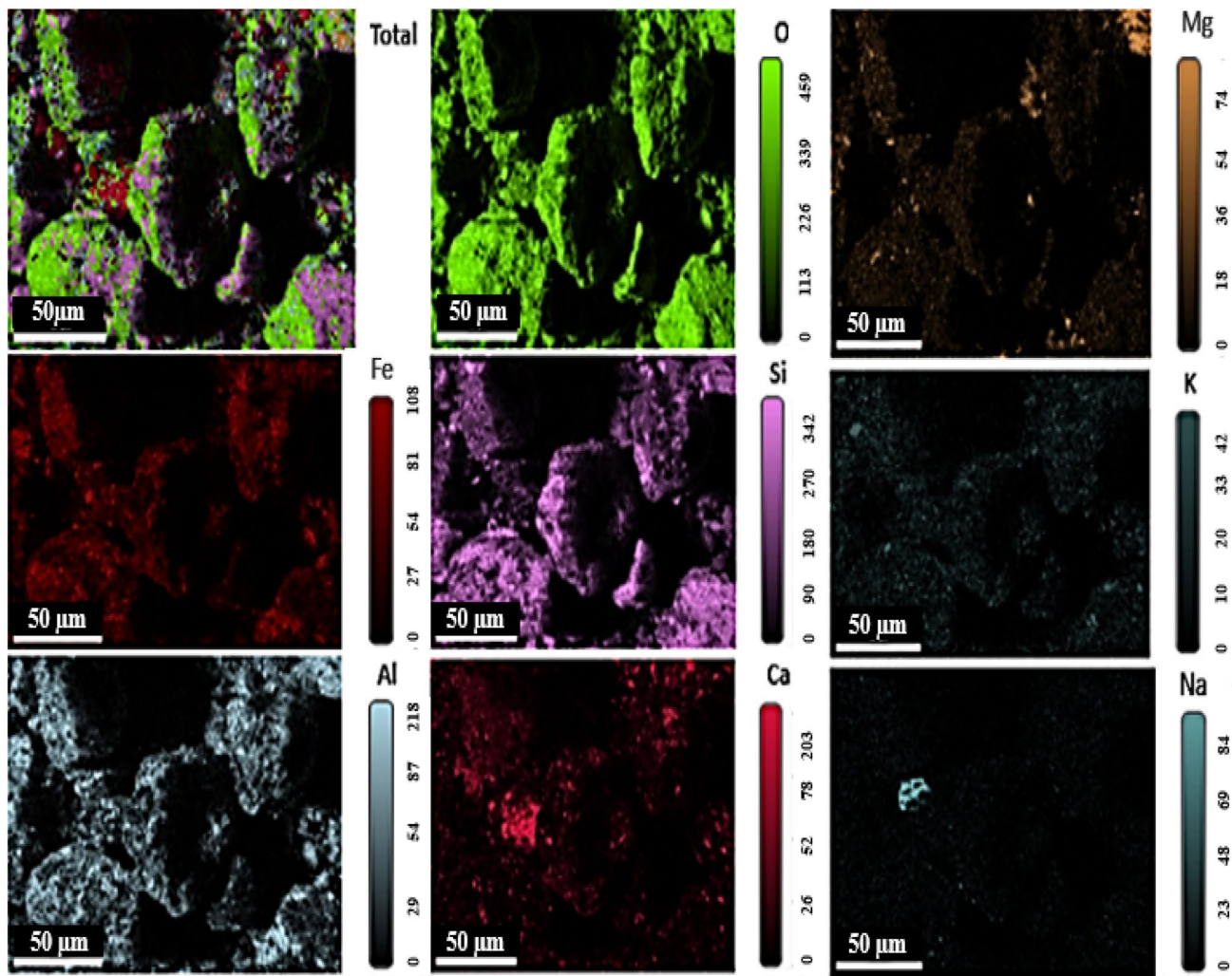


Fig. 5 ToF-SIMS imaging of NSR

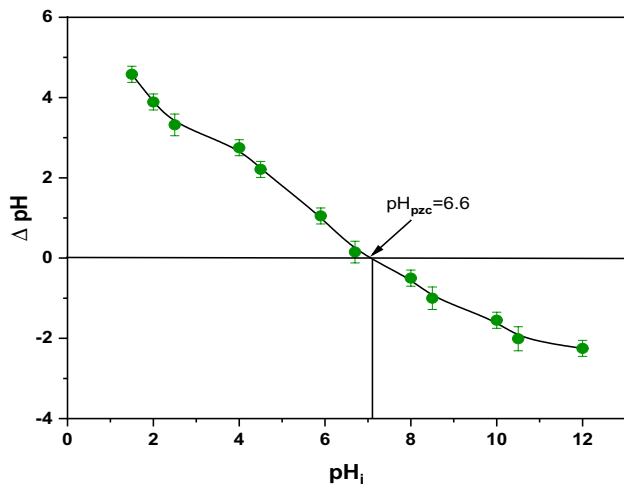


Fig. 6 PZC plot of NSR

3.1.7 Physico-Chemical Properties of Adsorbents

Other physicochemical properties of NSR sample like cation exchange capacity (CEC), porosity and moisture were studied. The measurement of the cationic exchange capacity of adsorbents is important since it allows the prediction of the adsorption mechanism of cationic pollutants. The CEC result is in agreement complement with the physicochemical characterizations of the adsorbents previously determined. A high CEC value of $148 \text{ meq } 100 \text{ g}^{-1}$ was noted for NSR, which justifies its swelling character. The porosity can be defined as the percentage of the total volume of materials that is taken up by pores. Hence, porosity is defined as the ratio between the volume of voids and the total volume of a porous medium. In this study, the porosity was affected by the mercury intrusion porosimeter method recorded on Quantachrome mercury POREMASTER. NSR was characterized by a large porosity of 90%, which is due to the

presence of pores in the structures of this adsorbent. Furthermore, Moisture measurement consists of determining the mass of water removed by drying with a moisture analyzer, the results of the moisture is low 1.05%, which explains the non-hygroscopic character of NSR.

3.2 Optimization of Adsorption Conditions

The variation of competitive adsorption of Cd (II), Cr (VI), and As (III) with different contact times was shown in Fig. 7a. The competitive removal of Cd (II), Cr (VI), and As (III) increased with time to obtain equilibrium around 30 min for Cr (VI), and As (III), and 40 min for Cd (II). The competitive removal of Cd (II), Cr (VI), and As (III) was rapid at first, which may be explained by the availability of active sites on the NSR surface and then these sites are saturated over time by the Cd (II), Cr (VI) and As (III) ions resulting in low adsorption capacity. Therefore, the difference in recovery efficiency of the multi-metals Cd (II), Cr (VI), and As (III) may be due to different ion exchanges between the metals and the surface load of NSR.

The influence of NSR mass on the performance of competitive removal of Cd (II), Cr (VI), and As (III) was investigated. Figure 7b proves that the recovery yield of Cd (II), Cr (VI), and As (III) increases with the increase in the capacity of NSR, which is probably attributed to the accessibility of extra-active sites on the surface of NSR. The optimal mass of NSR for the maximum competitive removal of Cd (II) was 0.7 g, while for Cr (VI) was 0.5 g, and around 0.3 g for As (III). Then, when the doses of NSR exceed this optimal mass the removal of Cd (II), Cr (VI), and As (III) becomes stable, which indicates the saturation of adsorption sites.

Therefore, Fig. 7c presents the effect of pH on the competitive adsorption of Cd (II), Cr (VI), and As (III) using NSR from the aqueous solution. This effect was evaluated in the pH range between 1 and 5 because the competitive adsorption process was not performed in the alkaline medium since the precipitation of Cd (II), Cr (VI), and As (III) metals as hydroxides. It was observed an increase in the pH of the solution from 2 to 5 with an increase in the removal of all the metals. From the results, it was evident that the best Cd (II) adsorption yield was obtained at 2.5 and 3 for Cr (VI) and As (III), respectively. The multi-metals adsorption process was elevated in the acid medium, it can be suggested that the adsorption process was via the non-electrostatic mechanism since the PZC value of NSR was higher than the obtained pH, indicating that the NSR surface was positive. Therefore, the most dominant mechanisms in the adsorption of Cd (II), Cr (VI), and As (III) using NSR can be designated by several physicochemical forces including the ion exchange, the complexation, and the precipitation. Various research in the literature reported the non-electrostatic mechanisms [16–19].

The effect of the initial concentration on the competitive adsorption yield of Cd (II), Cr (VI), and As (III) using NSR from the aqueous solution was exposed in Fig. 7d. The removal efficiency was found to be maximum at the initial concentration of 60 mg L⁻¹ for Cd (II), Cr (VI), and As (III). It can be resolved that adsorption efficiency increases with increasing initial concentration until saturation. These results may be explained by the existence of sufficient adsorption sites for NSR at lower initial concentrations. However, at higher concentrations, the Cd (II), Cr (VI), and As (III) ions were more numerous than the adsorption sites.

The influence of temperature on the removal of Cd (II), Cr (VI), and As (III) ions by NSR was presented in Fig. 7e. The results indicate that the competitive recovery capacity of Cd (II), Cr (VI), and As (III) ions were more favorable at 25 °C such as was decreased with increasing temperature for all the metals. This phenomenon suggests that the multi-metal removal of Cd (II), Cr (VI), and As (III) ions onto NSR was controlled by an exothermic reaction.

3.3 Adsorption Kinetic Study

The adsorption kinetic study was evaluated to measure the maximum adsorbed capacity as a function of time and to evaluate the mechanism of solute attachment to the adsorbent surface.

In this study, the linear and the nonlinear models of the pseudo-first-order (PFO), pseudo-second-order (PSO), and the linear intra-particle diffusion were used to describe the adsorption mechanism of Cd (II), Cr (VI), and As (III) ions by NSR [20, 21].

The nonlinear and linear forms of PFO model were presented by the following Eqs. 2, and 3 respectively:

$$Q_t = (Q_e - e^{-K_1 t}) \quad (2)$$

$$\ln(Q_e - Q_t) = \ln(Q_e) - K_1 t \quad (3)$$

The nonlinear and linear pseudo-second-order models were defined by the ensuing Eqs. 4, and 5 respectively:

$$Q_t = \frac{K_2 Q_e^2 t}{1 + K_2 Q_e t} \quad (4)$$

$$\frac{t}{Q_t} = \frac{1}{K_2 Q_e^2} + \frac{1}{Q_e} t \quad (5)$$

The intra-particle diffusion model was proposed by Weber and Morris in the next equation:

$$Q_t = K_w t^{\frac{1}{2}} + C \quad (6)$$

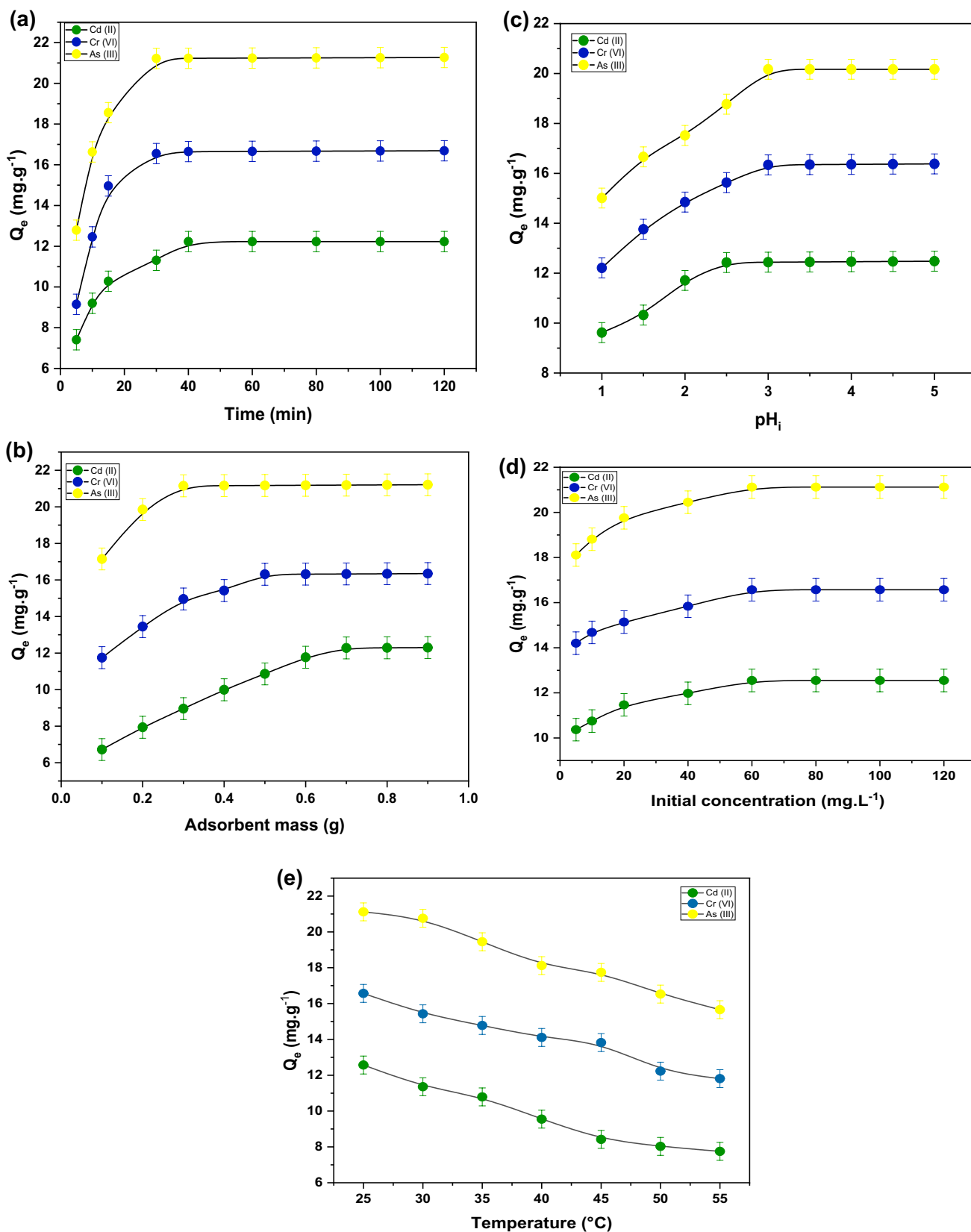


Fig. 7 Effects parameters of Cd (II), Cr (VI), and As (III) adsorption on NSR, **a** contact time, **b** NSR mass, **c** pH_i of the solution, and **d** initial metals concentration **e** temperature (pH=2.5 for Cd (II), and 3 for Cr (VI) and As (III))

where Q_t is the amount of adsorbed in time t (mg g^{-1}), Q_e is the adsorption capacity at equilibrium (mg g^{-1}), K_1 is the pseudo-first-order rate constant (min^{-1}), K_2 is the pseudo-second-order rate constant ($\text{g mg}^{-1} \text{min}^{-1}$), and K_w is the intra-particle diffusion rate constant ($\text{g mg}^{-1} \text{min}^{-1/2}$).

The linear and non-linear forms of the kinetic models are shown in Fig. 8, and the parameter values are listed in Table 2. The linearized PFO and PSO were the most widely used to describe the kinetics models of the competitive adsorption of Cd (II), Cr (VI), and As (III) ions onto NSR. According to the correlation coefficient (R^2) values, it was observed that the linear models of PFO and PSO are the most suitable for the adsorption process [22–24]. Based on the analysis results, the adsorption of Cd (II), Cr (VI), and As (III) onto NSR adsorbent was better described by the pseudo-second-order kinetic model with a high correlation coefficient, and the experimental adsorption capacity Q_e ($Q_{e,\text{exp}}$) are closer to those of the calculated Q_e ($Q_{e,\text{cal}}$) values. This result shows that the adsorption of Cd (II), Cr (VI), and As (III) ions on NSR adsorbent is mainly dominated by chemical adsorption.

The pseudo-first-order and pseudo-second-order kinetic models give no information on the diffusion of the adsorption process. In this context, the intra-particle diffusion model was also used in the experimental kinetic data to fully understand the diffusion mechanism Fig. 8c. The norms of the external diffusion constant K , as well as those of (R^2) are given in Table 3. The multilinearity of Cd (II), Cr (VI), and As (III) adsorption on NSR suggests that the entire adsorption process can be separated into two phases. the rate constant (K) and the correlation coefficients (R^2) of the first step are higher than that of the second step, which indicates that the first step is related to mass transfer to the outside surface of NSR while the second step is related to intra-particle diffusion.

3.4 Adsorption Isotherms

Adsorption isotherm allows to describe the interaction adsorbent-adsorbate, determine the maximum adsorption capacity, and identify the type of adsorption. Two models were used in this study Freundlich and Langmuir [25].

Freundlich model is definite by the fact that the adsorbent surface is heterogenous with non-uniform energy distribution of adsorption sites on the surface. The nonlinear and linear forms of this model is expressed by the following Eqs. 7, and 8 respectively:

$$Q_e = K_F + C_e^{1/n} \quad (7)$$

$$\ln(Q_e) = \ln(K_F) + \frac{1}{n} \ln(C_e) \quad (8)$$

where Q_e is the quantity of adsorption (mg g^{-1}); K_F is the Freundlich constant which expresses the adsorption affinity;

C_e is the equilibrated concentration of the solute (mg L^{-1}) and $1/n$ is the Freundlich constant that reflects the adsorption intensity.

The Langmuir model supposes that the surface of the adsorbents is ideally uniform; all sites adsorption has the same adsorption properties and there are no interactions between the adsorbed solute and solution; adsorption is limited to the monolayer. The Langmuir model is indicated by the following nonlinear and linear Eqs. 9, and 10 respectively:

$$Q_e = \frac{K_L C_e}{1 + K_L C_e} \quad (9)$$

$$\frac{C_e}{Q_e} = \frac{1}{K_L Q_{\text{max}}} + \frac{C_e}{Q_{\text{max}}} \quad (10)$$

where K_L is the Langmuir constant and Q_{max} is the maximum amount of solute adsorption over the solid phase (mg g^{-1}).

The isotherm adsorption of Cd (II), Cr (VI), and As (III) onto NSR was studied according to optimized conditions. Experimental Cd (II), Cr (VI), and As (III) ions adsorption data fitted to select isotherm models are presented in Fig. 9 using the linear and nonlinear equations. The various constants of the two models were calculated and represented in Table 4. The simplest method for determining isotherm parameters is to transform the equations into the linear form to facilitate the calculation of the constants by applying linear regression. The linear model presents well-defined straight lines with high linear regression coefficients [26–28]. According to the (R^2) value, it could be deduced that the competitive adsorption of Cd (II), Cr (VI), and As (III) ions onto NSR were best fitted to the Langmuir model, indicating the adsorption of Cd (II), Cr (VI), and As (III) fixed on the homogenous surface as a monolayer, and the maximum monolayer adsorption capacity (Q_{max}) attained was 16.75 mg g^{-1} for Cr (VI), 21.45 mg g^{-1} for As (III), and 12.63 mg g^{-1} for Cd (II). The R_L value was found within the range $0 < R_L < 1$, revealing that the adsorption of Cd (II), Cr (VI), and As (III) onto NSR is favorable.

3.5 Thermodynamic Study

The study of the influence of temperature on Cd (II), Cr (VI), and As (III) ions adsorption onto NSR, provides information on the spontaneity of the adsorption process and the determination of parameters such as the variation of the standard enthalpy (ΔH°), the variation of the standard entropy (ΔS°), and the free energy (ΔG°) [21]. These standard thermodynamic characteristics were calculated by the following equations:

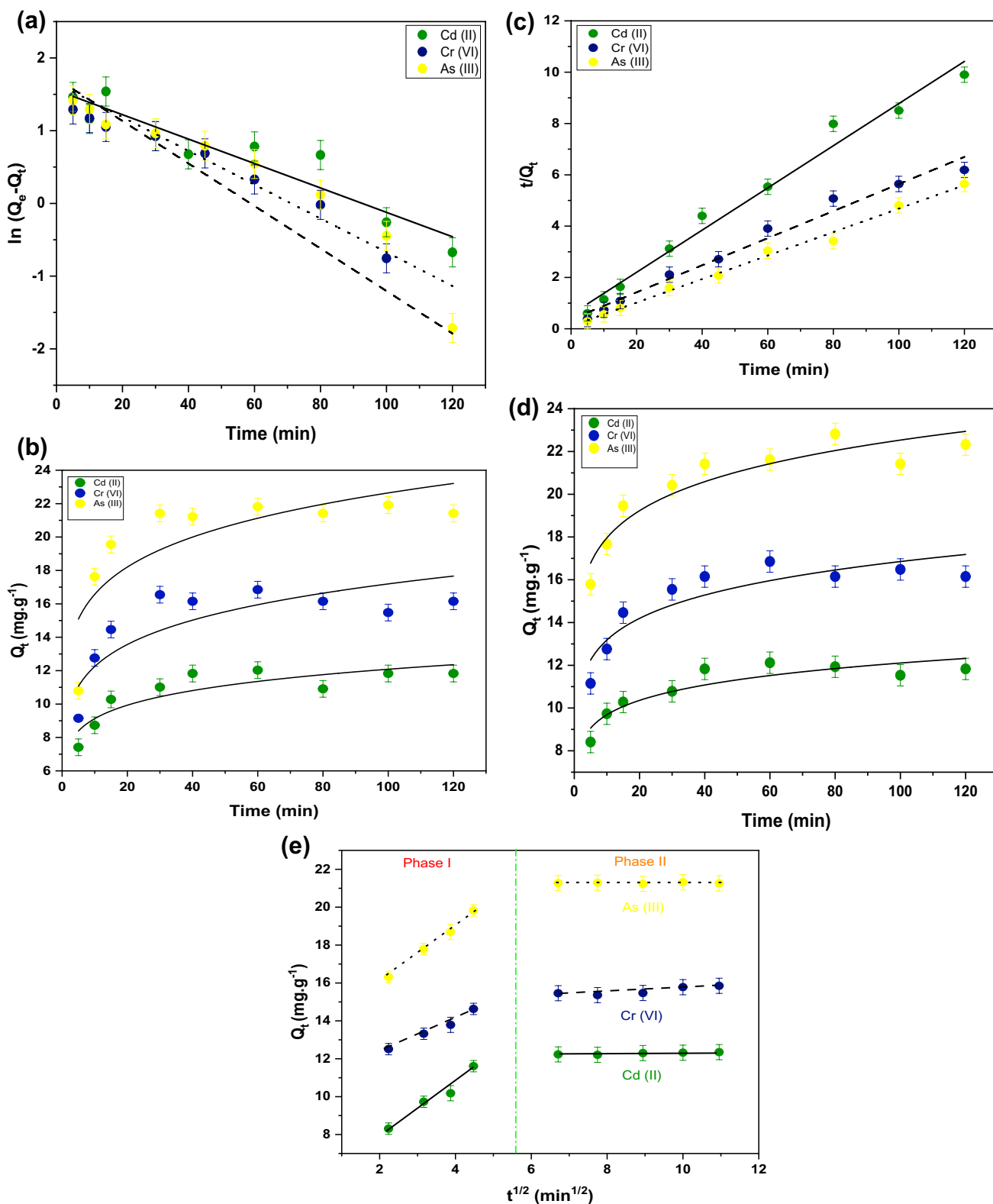


Fig. 8 Adsorption kinetic models **a**, **b** linear and nonlinear PFO, **c**, **d** linear and nonlinear PSO, and **e** IPD (pH=2.5 for Cd (II) and 3 for Cr (VI) and As (III))

Table 2 Kinetic constants for Cd (II), Cr (VI), and As (III) adsorption on NSR using linear and nonlinear forms (pH=2.5 for Cd (II), and 3 for Cr (VI) and As (III))

Metals	$Q_{e,exp}$ (mg g ⁻¹)	Pseudo-first-order			Pseudo-second-order		
		$Q_{e,cal}$ (mg g ⁻¹)	K_1 (min ⁻¹)	R^2	Q_e (mg g ⁻¹)	K_2 (g mg ⁻¹ min ⁻¹)	R^2
Linear							
Cd (II)	12.56	0.441	0.016	0.88	12.16	0.012	0.98
Cr (VI)	16.64	0.530	0.029	0.85	17.91	0.006	0.97
As (III)	21.23	0.897	0.023	0.91	21.83	0.014	0.99
Nonlinear							
Cd (II)	12.56	1.257	0.078	0.45	8.31	0.0143	0.61
Cr (VI)	16.64	2.015	0.081	0.35	12.53	0.0132	0.54
As (III)	21.23	2.758	0.065	0.38	18.62	0.017	0.68

Table 3 Intra-particle diffusion model for Cd (II), Cr (VI), and As (III) adsorption on NSR (pH=2.5 for Cd (II) and 3 for Cr (VI) and As (III))

Metals	Phase I			Phase II		
	K_1 (g mg ⁻¹ min ^{-1/2})	C (mg g ⁻¹)	R^2	K_2 (g mg ⁻¹ min ^{-1/2})	C (mg g ⁻¹)	R^2
Cd (II)	0.032	11.991	0.92	0.980	6.343	0.78
Cr (VI)	0.019	16.568	0.93	0.662	11.494	0.83
As (III)	0.009	21.266	0.95	0.794	15.429	0.87

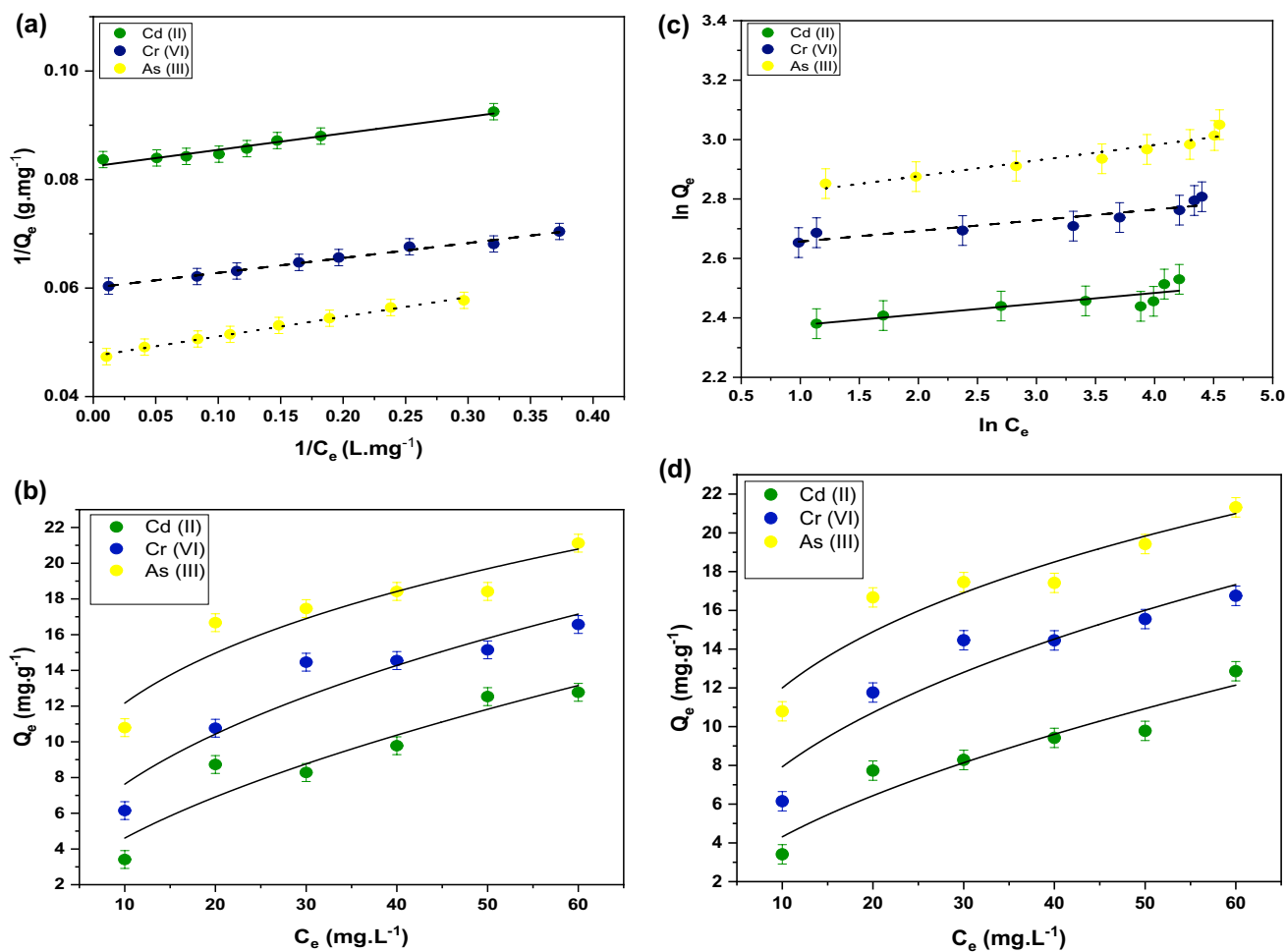


Fig. 9 Adsorption isotherm for removal of Cd (II), Cr (VI), and As (III) **a, b** linear and nonlinear Langmuir and **c, d** linear and nonlinear Freundlich models (pH=2.5 for Cd (II) and 3 for Cr (VI) and As (III))

Table 4 Adsorption isotherm constants for removal of Cd (II), Cr (VI), and As (III) using nonlinear and linear forms (pH=2.5 for Cd (II), and 3 for Cr (VI) and As (III))

Metals	Langmuir constants			Fruendlich constants		
	Q _{e,cal} (mg g ⁻¹)	R _L (L g ⁻¹)	R ²	K _F (mg g ⁻¹)	n	R ²
Linear						
Cd (II)	12.63	0.368	0.95	0.063	27.701	0.72
Cr (VI)	16.75	0.455	0.98	0.047	27.855	0.84
As (III)	21.45	0.764	0.99	0.019	19.048	0.91
Nonlinear						
Cd (II)	10.52	0.489	0.67	0.045	23.419	0.55
Cr (VI)	14.73	0.741	0.63	0.011	24.235	0.47
As (III)	19.82	0.954	0.70	0.001	15.56	0.39

$$\Delta G^\circ = -RT \left(\ln \frac{Q_e}{C_e} \right) \tag{11}$$

$$K_d = \frac{Q_e}{C_e} \tag{12}$$

$$\ln K_d = \frac{\Delta S^\circ}{R} - \frac{\Delta H^\circ}{RT} \tag{13}$$

where R is the perfect gas constant (8.314 J mol⁻¹ K⁻¹), T is the temperature in Kelvin (K) and K_d is the distribution coefficient of the solute in the adsorbent and the solution.

The thermodynamic parameters for the adsorption of Cd (II), Cr (VI), and As (III) onto NSR were summarized in Table 5. The negative values of ΔS° indicate a random increase at the adsorbents/solution interface during the competitive adsorption of Cd (II), Cr (VI), and As (III) onto NSR. Therefore, the negative values of ΔH° suggest that the interaction between Cd (II), Cr (VI), and As (III), and

NSR was an exothermic process. In addition, the free energy values were negative for all metals, therefore the competitive elimination of Cd (II), Cr (VI), and As (III) was spontaneous and thermodynamically favorable. It was noted that the values of ΔG° increase slightly with temperature reflecting the negative effect of temperature on Cd (II), Cr (VI), and As (III) competitive adsorption.

3.6 Regeneration of NSR

In addition, the adsorption efficiency and the regeneration of adsorbents, and their resistance to acid or base conditions have also been demonstrated as significant parameters for an ideal adsorbent. The competitive adsorption/desorption of Cd (II), Cr (VI), and As (III) and the regeneration of NSR by several acids for three cycles was presented in Fig. 10. The desorption of Cd (II) using nitric acid, sulfuric acid, and hydrochloric acid was achieved at 13%, 21%, and 40%, respectively. While, the percentage desorption of Cr (VI) was approximately 24% for nitric acid, 35% for sulfuric acid,

Table 5 Thermodynamic parameters for the adsorption of Cd (II), Cr (VI), and As (III) (pH=2.5 for Cd (II), and 3 for Cr (VI), and As (III))

Metals	Temperature (K)	ΔS° (KJ mol ⁻¹ K ⁻¹)	ΔH° (KJ .mol ⁻¹)	ΔG° (KJ mol ⁻¹)
Cd (II)	298	- 0.116	- 38.469	- 3.841
	300			- 3.609
	302			- 3.376
	304			- 3.144
	306			- 2.911
Cr (VI)	298	- 0.120	- 40.501	- 4.650
	300			- 4.410
	302			- 4.16
	304			- 3.928
	306			- 3.688
As (III)	298	- 0.296	- 94.272	- 5.944
	300			- 5.352
	302			- 4.759
	304			- 4.166
	306			- 3.573

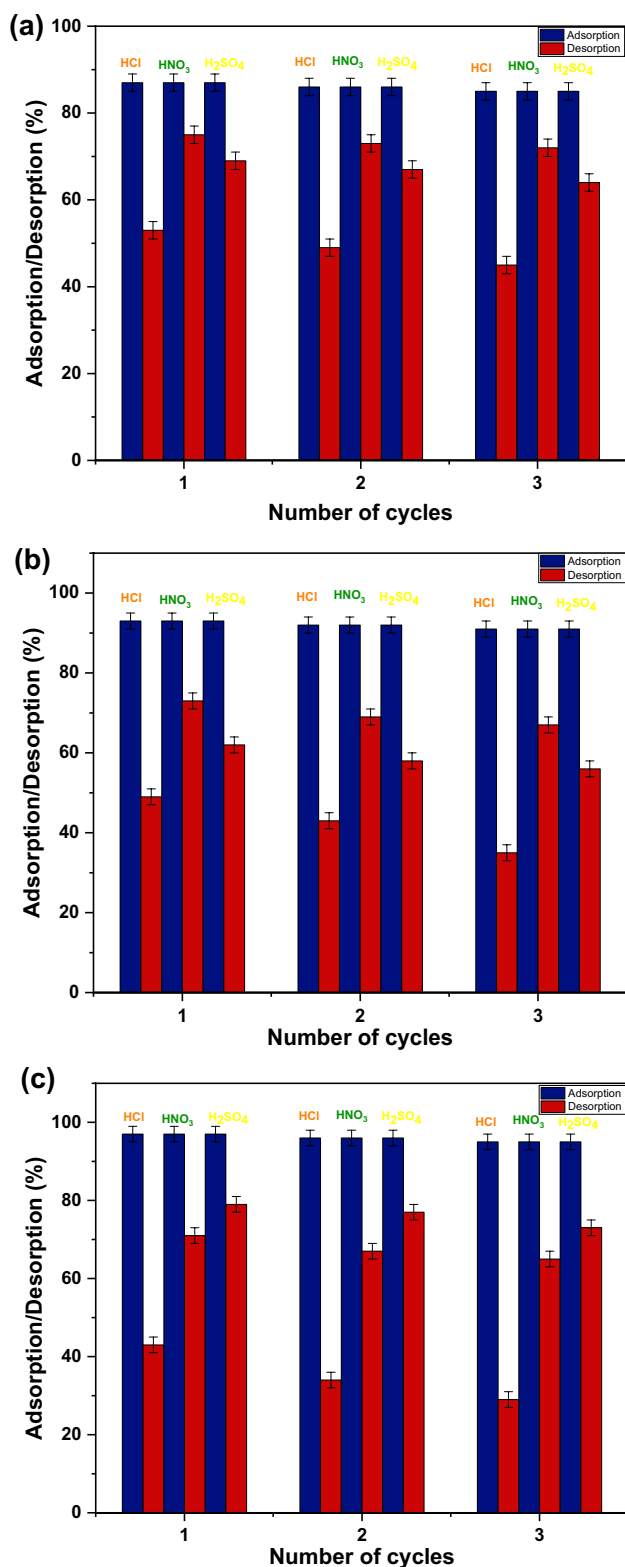


Fig. 10 The regeneration of NSR **a** Cd (II), **b** Cr (VI), and **c** As (III) (pH = 2.5 for Cd (II), and 3 for Cr (VI) and As (III))

and 56% for hydrochloric acid. Then, the desorption of As (III) was 30% for nitric acid, 22% for sulfuric acid, and 66% for hydrochloric acid. It was evident that hydrochloric acid was the most effective in the desorption of Cd (II), Cr (VI), and As (III) from the aqueous solution. The regeneration efficiency of NSR was probably due to the acidity force of hydrochloric acid, which can be easily broken the chemical bond between Cd (II), Cr (VI), and As (III), and the functional grouping of the NSR surface. According to the results, the competitive adsorption capacity has not much changed, this explains that NSR has an excellent regeneration capability, and it can be limited to the moderate strength of the competitive adsorption process or the excellent surface allocation to Cd (II), Cr (VI), and As (III).

3.7 Mechanism of Multi-metals Adsorption on NSR

To understand and demonstrate the competitive removal mechanism of Cd (II), Cr (VI), and As (III) ions onto NSR, the XRD, FTIR, AFM, and SEM before and after adsorption were investigated and compared to explore the possible interaction sites between the adsorbent and adsorbate molecule.

The XRD spectrums of NSR after contacting with Cd (II), Cr (VI), and As (III) ions were recorded and compared with NSR before adsorption (Fig. 11a). The patterns designate that there are no new characteristic peaks appeared. Consequently, the interlamellar distance of the founded phases remains unchanged before and after the recovery of Cd (II), Cr (VI), and As (III) onto NSR. These observations suggest that Cd (II), Cr (VI), and As (III) removal was affected by the bond between metal ions and the positively charged surface of NSR. This result explains the difficulty of exchanging intercalated ions in NSR layers and Cd (II), Cr (VI), and As (III).

The FTIR spectra in Fig. 11b demonstrates functional groups on the surface of NSR before and after the competitive removal of Cd (II), Cr (VI), and As (III). It was observed that the FTIR spectra before and after the recovery of metal ions onto NSR were almost similar with a significant difference in absorbance, indicating that all functional groups participated in the adsorption process. The difference in absorbances was attributed to the change in Cd (II), Cr (VI), and As (III) associated with anionic functional groupings, suggesting that these groupings were the predominant contributors to Cd (II), Cr (VI), and As (III) removal.

The textural and morphological properties of the NSR surface were studied using the SEM (Fig. 11c, d). The SEM photographs of NSR after removal of Cd (II), Cr (VI), and As (III) detect more dense agglomerates than NSR before the adsorption process. It was also noted that the particle size was larger which shows that a great amount of Cd (II), Cr (VI), and As (III) was attached to the surface of NSR.

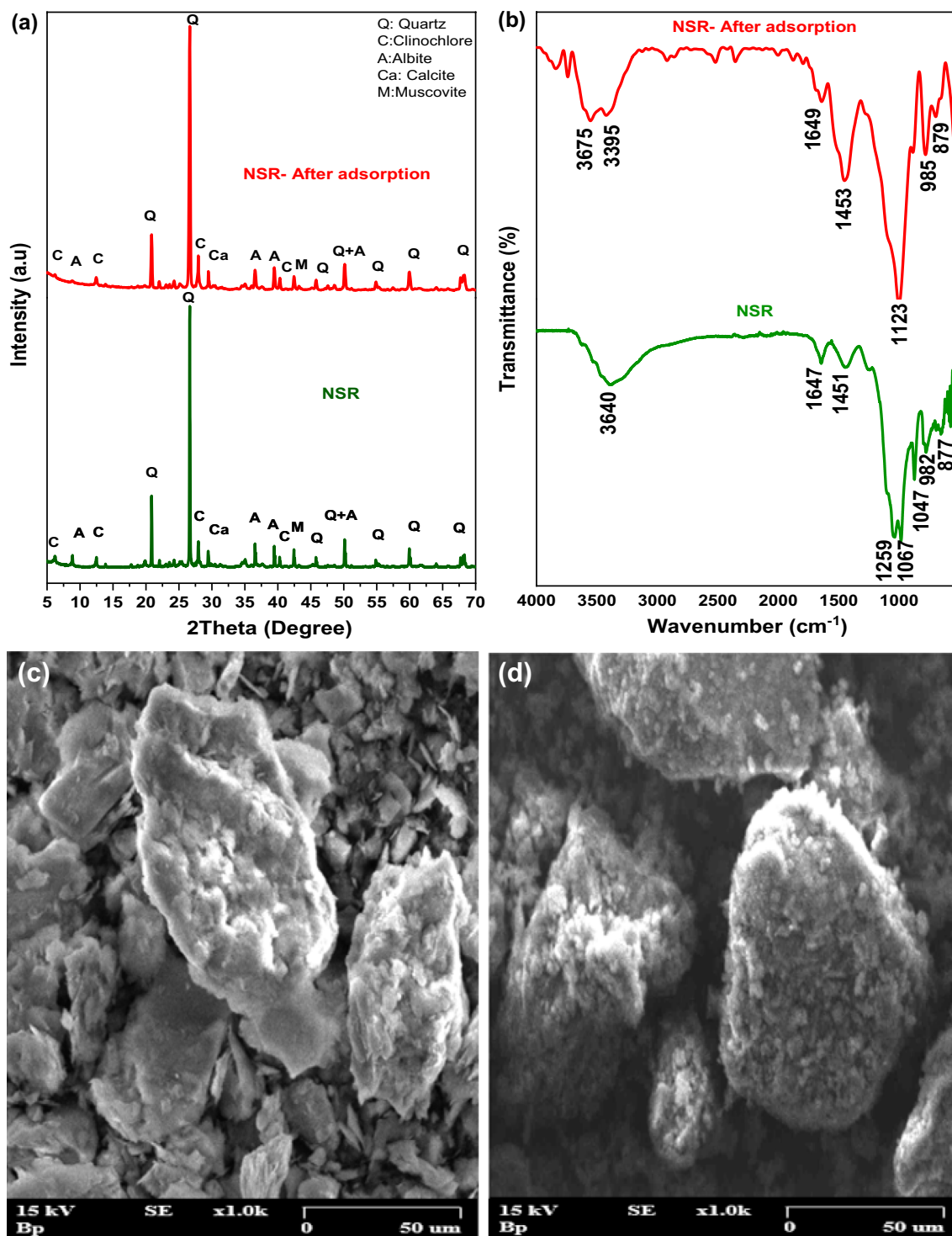


Fig. 11 Characterization of NSR before and after the adsorption **a** XRD, **b** FTIR, **c**, **d** SEM, and **e**, **f** AFM (pH=2.5 for Cd (II), and 3 for Cr (VI) and As (III))

To confirm the NSR binding sites, AFM measurements of the NSR surface before and after the competitive removal of Cd (II), Cr (VI), and As (III) were performed (Fig. 11e, f). The many smaller branches at the NSR surface and the size

of the different particles inside NSR show the distribution of the surface roughness height before the adsorption process. On the other hand, after the recovery of Cd (II), Cr (VI), and As (III) most of the sites responsible for the adsorption of

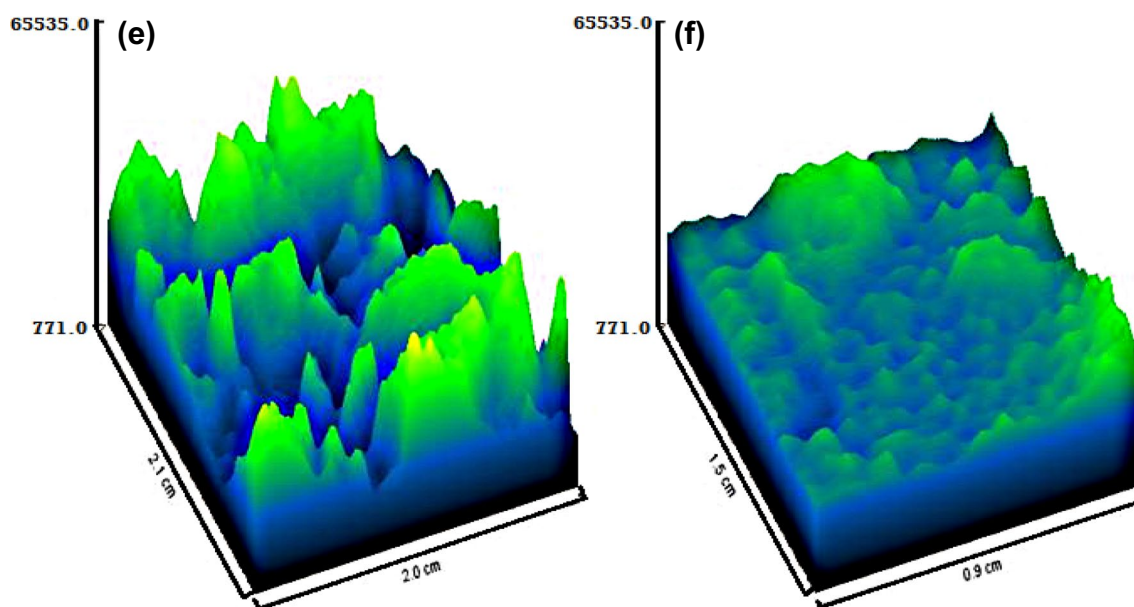


Fig. 11 (continued)

Cd (II), Cr (VI), and As (III) were located on the extremities of the branches on the surface of the NSR. It suggests that the ions exchanges between sorption sites and functional groups and Cd (II), Cr (VI), and As (III) ions were the main mechanism responsible for the sorption process of the NSR.

3.8 Comparative Study

This study aims to analyze the difference in removal capacities of heavy metals using NSR and other adsorbents. Table 6 lists the maximum adsorption capacities and the

removal yields of heavy metals by several adsorbents. In this study, the removal capacity of As (III) was higher than Cr (VI) and Cd (II). It was observed that the NSR adsorption amount was relatively higher than numerous studies published in recent years [29–31]. The differences in the adsorption capacities of heavy metals by natural adsorbents can be attributed essentially to differences in the physicochemical parameters of each adsorbent, including cationic exchange capacities, the specific surface area, and their rich grouping of functional surfaces and their structures. Therefore, NSR without any treatment shows the excellent recovery of heavy

Table 6 Comparison of the competitive adsorption capacities of several adsorbents

Adsorbent	Pollutant	Removal rate (%)	Q_{\max} (mg g ⁻¹)	References
Natural clay southern Tunisia	Pb (II)	99	16.43	[32]
	Cd (II)	98	13	
	Zn (II)	95	9	
	Cu (II)	98	11.45	
Calcined natural clay	Pb (II)	98	23.91	[33]
	Cd (II)	99	16.7	
	Cr (VI)	99	11.2	
Shanghai Silty clay	Cd (II)	99	8.90	[34]
	Pb (II)	99	26.46	
	As (V)	95	2.83	
	Cr (VI)	97	1.85	
Tanzanian Malangali kaolin	Cd (II)	97	1.067	[7]
	Co (II)	95	1.043	
Silty clay	Ni (II)	96	3.60	[35]
	Cd (II)	93	5.48	
NSR	Cd (II)	95	12.63	This work
	Cr (VI)	98	16.75	
	As (III)	99	21.45	

metals, suggesting that it is suitable for practical engineering applications.

4 Conclusion

In the present study, Moroccan Middle Atlas rock was characterized and tested without physical and/or chemical treatments for the removal of multi-metals Cd (II), Cr (VI), and As (III) from aqueous solution. The competitive adsorption of Cd (II), Cr (VI), and As (III) onto NSR was investigated by the batch experimental method using the optimal conditions. The best fit of the kinetic data was obtained by the linear pseudo-second-order kinetic model, indicating that the adsorption mechanism was controlled by chemisorption. For the isotherm data, the linear Langmuir model was more appropriate for the adsorption process than the Freundlich model, indicating the homogeneities of the active sites on the surface of NSR, and the maximum monolayer adsorption capacities of Cd (II), Cr (VI), and As (III) were found to be 12.63 mg g⁻¹, 16.75 mg g⁻¹, and 21.45 mg g⁻¹, respectively. Thermodynamic values showed that the adsorption process was exothermic, favorable, and spontaneous in nature. The competitive removal of Cd (II), Cr (VI), and As (III) on NSR was confirmed by various characterization techniques including XRD, FTIR, and SEM analysis. According to the obtained results in this study, this natural rock can be considered as an eco-friendly and low-cost alternative adsorbent to effectively remove Cd (II), Cr (VI), and As (III) ions compared to other raw adsorbents reported in the literature, suggesting a possible application in industrial wastewater treatment.

Acknowledgements This work has been possible by following the assist of several people. All thanks to the authors for their collaboration and excellent articles, for their precious help, their patience, and their proofreading and corrections. Thanks to everyone who helped and contributed to the development of this research.

Data Availability The datasets used and analyzed during the current study are available from the corresponding author upon request.

Declarations

Conflict of interest The authors declare that they have no known competing financial interests or personal relationships that could have appeared to influence the work reported in this paper.

References

- Bissen M, Frimmel FH (2003) Arsenic—a review. Part I: occurrence, toxicity, speciation, mobility. *Acta Hydrochim Hydrobiol* 31(1):9–18. <https://doi.org/10.1002/ahch.200390025>
- Amin N, Hussain A, Alamzeb S, Begum S (2013) Accumulation of heavy metals in edible parts of vegetables irrigated with waste water and their daily intake to adults and children, District Mardan, Pakistan. *Food Chem* 136(3–4):1515–1523. <https://doi.org/10.1016/j.foodchem.2012.09.058>
- An N, Zagorščak R, Thomas HR (2022) Adsorption characteristics of rocks and soils, and their potential for mitigating the environmental impact of underground coal gasification technology: a review. *J Environ Manage* 305:114390. <https://doi.org/10.1016/j.jenvman.2021.114390>
- Xing Y, Jiang Y, Liu S, Tan S, Luo X, Huang Q, Chena W (2022) Surface corrosion by microbial flora enhances the application potential of phosphate rock for cadmium remediation. *Chem Eng J* 429:132560. <https://doi.org/10.1016/j.cej.2021.132560>
- Budianta W (2021) The influence of mineralogical composition on the adsorption capacity of heavy metals solution by java natural clay Indonesia. *ASEAN Eng J* 11(2):64–76
- Abbou B, Ouaddari H, Elkhatabi O, Habsaoui A, Lebkiari A, El Housseine RIFI (2021) Removal of Cd(II), Cu(II), and Pb(II) by adsorption onto natural clay: a kinetic and thermodynamic study. *Turk J Chem.* <https://doi.org/10.18596/jotcsa.882016>
- Malima N, Owonubi S, Lugwisha E (2021) Thermodynamic, isothermal and kinetic studies of heavy metals adsorption by chemically modified Tanzanian Malangali kaolin clay. *Int J Environ Sci Technol.* <https://doi.org/10.1007/s13762-020-03078-0>
- Belhabra M, Zerraf S, Kheireddine A, Altomare A, Tridane M, Ouasri A, Radid M, Belaouad S (2018) Structural and vibrational study of diphenylhydrazine dihydrogenophosphate single crystal (C₆H₉N₂)₂H₂P₂O₇ (DPHDP). *Chem Data Collect* 13–14:73–83. <https://doi.org/10.1016/j.cdc.2018.01.002>
- Atibi A, Kababi K, Mustafa B, Zerraf S, Tridane M, Belaouad S (2018) Chemical preparation, crystal structure and vibrational study of a new dihydrogenotriphosphate trihydrate of 4-aminobenzoic acid fertilizer type NP. *J Coord Chem* 71:1–18. <https://doi.org/10.1080/00958972.2018.1528579>
- Jarmouni N, Tomaiuolo M, Gabbani A, Pineider F, Bassam R, Belaouad S, Benmokhtar S (2021) Synthesis of brightly luminescent colloidal formamidinium lead bromide perovskite FAPbBr₃ nanoplatelets with tunable emission. *MATEC Web Conf* 348:01015. <https://doi.org/10.1051/mateconf/202134801015>
- Bassam R, El Alouani M, Maissara J, Rachdi Y, Jarmouni N, Khattabi EHE, Chbihi MEM, Belaouad S (2022) Physico-chemical characterization of natural rocks and their valorization on the removal of arsenic from aqueous solution. *Mater Today Proc.* <https://doi.org/10.1016/j.matpr.2021.12.498>
- Bassam R, El Alouani M, Maissara J, Jarmouni N, Belhabra M, Chbihi MEM, Belaouad S (2021) Investigation of competitive adsorption and desorption of heavy metals from aqueous solution using raw rock: Characterization kinetic, isotherm, and thermodynamic. *Mater Today Proc.* <https://doi.org/10.1016/j.matpr.2021.11.450>
- Bassam R, El Alouani M, Maissara J, Jarmouni N, Belhabra M, Chbihi MEM, Belaouad S (2022) Enhanced removal of cadmium ions using Moroccan natural clays: characterization, kinetic, isotherm, thermodynamic, and regeneration investigations. *Mater Today Proc.* <https://doi.org/10.1016/j.matpr.2022.02.536>
- Calvete JJ, Sanz L, Angulo Y, Lomonte B, Gutiérrez JM (2009) Venoms, venomics, antivenomics. *FEBS Lett* 583(11):1736–1743. <https://doi.org/10.1016/j.febslet.2009.03.029>
- Korolev VA, Nesterov DS (2018) Regulation of clay particles charge for design of protective electrokinetic barriers. *J Hazard Mater* 358:165–170. <https://doi.org/10.1016/j.jhazmat.2018.06.023>
- Qu C, Chen W, Hu X, Cai P, Chen C, Yu XY, Huang Q (2019) Heavy metal behaviour at mineral-organo interfaces: mechanisms, modelling and influence factors. *Environ Int* 131:104995. <https://doi.org/10.1016/j.envint.2019.104995>

17. Chen Q, Zheng J, Xu J, Dang Z, Zhang L (2019) Insights into sulfamethazine adsorption interfacial interaction mechanism on mesoporous cellulose biochar: Coupling DFT/FOT simulations with experiments. *Chem Eng J* 356:341–349. <https://doi.org/10.1016/j.cej.2018.09.055>
18. Khan MA, Khan S, Ding X, Khan A, Alam M (2018) The effects of biochar and rice husk on adsorption and desorption of cadmium on to soils with different water conditions (upland and saturated). *Chemosphere* 193:1120–1126. <https://doi.org/10.1016/j.chemosphere.2017.11.110>
19. Ahmad SZN, Wan Salleh WN, Ismail AF, Yusof N, Mohd Yusop MZ, Aziz F (2020) Adsorptive removal of heavy metal ions using graphene-based nanomaterials: toxicity roles of functional groups and mechanisms. *Chemosphere* 248:126008. <https://doi.org/10.1016/j.chemosphere.2020.126008>
20. El Alouani M, Saufi H, Moutaoukil G, Alehyen S, Nematollahi B, Belmaghraoui W, Taibi M (2021) Application of geopolymers for treatment of water contaminated with organic and inorganic pollutants: State-of-the-art review. *J Environ Chem Eng* 9(2):105095. <https://doi.org/10.1016/j.jece.2021.105095>
21. Saufi H, Alouani ME, Aride J, Taibi M (2020) Rhodamine B biosorption from aqueous solution using *Eichhornia crassipes* powders: isotherm, kinetic and thermodynamic studies. *Chem Data Collect* 25:100330. <https://doi.org/10.1016/j.cdc.2019.100330>
22. Xiao Y, Azaiez J, Hill JM (2018) Erroneous application of pseudo-second-order adsorption kinetics model: ignored assumptions and spurious correlations. *Ind Eng Chem Res* 57(7):2705–2709. <https://doi.org/10.1021/acs.iecr.7b04724>
23. López-Luna J, Montes LER, Vargas SM, Martínez AI, Ricardoz OFM, González-Chávez MCA, Carrillo-González R, Solís-Domínguez FA, del Carmen Cuevas-Díaz M, Vázquez-Hipólito V (2019) Linear and nonlinear kinetic and isotherm adsorption models for arsenic removal by manganese ferrite nanoparticles. *SN Appl Sci* 1(8):950. <https://doi.org/10.1007/s42452-019-0977-3>
24. Grzesik M, Szymonski KA (2021) Comment on “erroneous application of pseudo-second-order adsorption kinetics model: ignored assumptions and spurious correlations.” *Ind Eng Chem Res* 60(24):8957–8959. <https://doi.org/10.1021/acs.iecr.1c01663>
25. Alouani ME, Alehyen S, Achouri ME, Taibi M (2017) Potential use of moroccan fly ash as low cost adsorbent for the removal of two anionic dyes (indigo carmine and acid orange). *Journal of Materials and Environmental Sciences* 8:3397–3409
26. Chen X (2015) Modeling of experimental adsorption isotherm data. *Information*. <https://doi.org/10.3390/info6010014>
27. Hamzaoui M, Bestani B, Benderdouche N (2018) The use of linear and nonlinear methods for adsorption isotherm optimization of basic green 4-dye onto sawdust-based activated carbon. *Journal of Material Environmental Science*. 9:1110–1118
28. Ayawei N, Ebelegi AN, Wankasi D (2017) Modelling and interpretation of adsorption isotherms. *J Chem* 2017:e3039817. <https://doi.org/10.1155/2017/3039817>
29. Bassam R, El Alouani M, Maissara J, Rachdi Y, Jarmouni N, Khattabi EHE, Chbihi MEM, Belaouad S (2021) Studies on the removal of cadmium toxic metal ions by natural clays from aqueous solution by adsorption process. *J Chem* 2021:e7873488. <https://doi.org/10.1155/2021/7873488>
30. Ghorbel-Abid I, Trabelsi-Ayadi M (2015) Competitive adsorption of heavy metals on local landfill clay. *Arab J Chem* 8(1):25–31. <https://doi.org/10.1016/j.arabjc.2011.02.030>
31. Xu H, Yuan H, Yu J, Lin S (2019) Study on the competitive adsorption and correlational mechanism for heavy metal ions using the carboxylated magnetic iron oxide nanoparticles (MNPs-COOH) as efficient adsorbents. *Appl Surf Sci* 473:960–966. <https://doi.org/10.1016/j.apsusc.2018.12.006>
32. Khalfa L, Sdiri A, Bagane M, Cervera ML (2020) Multi-element modeling of heavy metals competitive removal from aqueous solution by raw and activated clay from the Aleg formation (Southern Tunisia). *Int J Environ Sci Technol* 17(4):2123–2140. <https://doi.org/10.1007/s13762-019-02614-x>
33. Khalfa L, Sdiri A, Bagane M, Cervera ML (2021) A calcined clay fixed bed adsorption studies for the removal of heavy metals from aqueous solutions. *J Clean Prod* 278:123935. <https://doi.org/10.1016/j.jclepro.2020.123935>
34. Korake SR, Jadhao PD (2021) Investigation of Taguchi optimization, equilibrium isotherms, and kinetic modeling for cadmium adsorption onto deposited silt. *Heliyon* 7(1):e05755. <https://doi.org/10.1016/j.heliyon.2020.e05755>
35. Samad A, Din MI, Ahmed M (2020) Studies on batch adsorptive removal of cadmium and nickel from synthetic waste water using silty clay originated from Balochistan–Pakistan. *Chin J Chem Eng* 28(4):1171–1176. <https://doi.org/10.1016/j.cjche.2019.12.016>